



HAL
open science

Transmission electron microscopy in situ investigation of dislocation behaviour in semiconductors and the influence of electronic excitation

Suzel Lavagne, Colette Levade, Guy Vanderschaeve

► To cite this version:

Suzel Lavagne, Colette Levade, Guy Vanderschaeve. Transmission electron microscopy in situ investigation of dislocation behaviour in semiconductors and the influence of electronic excitation. *Philosophical Magazine*, 2006, 86 (29-31), pp.4923-4940. 10.1080/14786430600750038 . hal-00513708

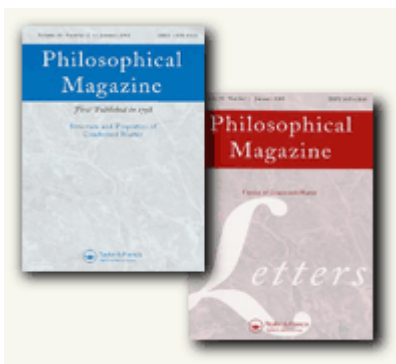
HAL Id: hal-00513708

<https://hal.science/hal-00513708>

Submitted on 1 Sep 2010

HAL is a multi-disciplinary open access archive for the deposit and dissemination of scientific research documents, whether they are published or not. The documents may come from teaching and research institutions in France or abroad, or from public or private research centers.

L'archive ouverte pluridisciplinaire **HAL**, est destinée au dépôt et à la diffusion de documents scientifiques de niveau recherche, publiés ou non, émanant des établissements d'enseignement et de recherche français ou étrangers, des laboratoires publics ou privés.



Transmission electron microscopy in situ investigation of dislocation behaviour in semiconductors and the influence of electronic excitation

Journal:	<i>Philosophical Magazine & Philosophical Magazine Letters</i>
Manuscript ID:	TPHM-06-Jan-0012.R2
Journal Selection:	Philosophical Magazine
Date Submitted by the Author:	06-Apr-2006
Complete List of Authors:	Lavagne, Suzel; CEMES/CNRS; Altis Semiconductor Levade, Colette; INSA, Physics; CEMES/CNRS Vanderschaeve, Guy; INSA, Physics; CEMES /CNRS
Keywords:	dislocation dynamics, electron microscopy, strained layers
Keywords (user supplied):	Semiconductor compounds



1
2
3
4 **Transmission electron microscopy *in situ* investigation of dislocation**
5 **behaviour in semiconductors and the influence of electronic excitation**
6
7
8
9

10
11
12
13
14 S. LAVAGNE[†], C. LEVADE and G. VANDERSCHAEVE*

15
16
17
18 CEMES/CNRS, BP 94347 31055 Toulouse, France

19
20 and INSA Physics Department, av. de Rangueil, 31077 Toulouse, France
21
22
23
24
25
26

27 *In situ* straining experiments in a transmission electron microscope provide a unique
28 way to investigate in real time the influence of various parameters (temperature,
29 electron beam intensity, ...) on the dislocation behaviour in semiconductors. A
30 systematic study of the influence of electronic excitation on the dislocation behaviour
31 in single phase ZnS crystals is reported. The observed radiation enhanced dislocation
32 motion is attributed to a lowering of the lattice friction, due to non radiative
33 recombination of carriers at electronic levels associated with dislocations. Analysis of
34 the results makes it possible to determine which elementary mechanism of dislocation
35 glide is affected by this effect. The defect dynamics in a ZnSe/GaAs heterostructure in
36 the course of *in situ* heating experiments is investigated. Different dislocation
37 mechanisms are analysed, which emphasize the influence of electronic excitation on
38 the dislocation behaviour. The contribution of these mechanisms to the strain
39 relaxation is discussed.
40
41
42
43
44
45
46
47
48
49
50
51
52

53
54
55 *Keywords:* Semiconductor compounds; Dislocation dynamics; Electron microscopy;
56
57 Strained layers
58
59
60

[†] present address: Altis Semiconductors 224 Bd John Kennedy, 91105 Corbeil Essonnes, France

* corresponding author

1. Introduction

In the low to medium temperature range, moving dislocations in solids with covalent or ionocovalent bonding experience a high lattice friction. This results in a thermally activated motion which, in the appropriate temperature range, could be observed in real time during *in situ* experiments in a transmission electron microscope (TEM). These experiments make a thorough determination of activation parameters possible. By comparison with other techniques, for example double etching, X-ray topography (for a review, see [1, 2]), where dislocation velocities are averaged over travel distances of a few tenths of a micrometer, the *in situ* TEM investigation makes possible an analysis of the behaviour of short dislocation segments in the early stages of source operation. Results are available on elemental semiconductors, III-V and II-VI compounds [3]. In these crystals, the dislocation movement is well described by the Peierls mechanism (nucleation and propagation of kink pairs).

In a number of large band gap semiconductors the behaviour of lattice defects is strongly influenced by light illumination (photoplastic effect) or electron beam irradiation (cathodoplastic effect). These effects are related to the special properties of dislocations in these materials. Indeed they provide electronic levels in the band gap and act as active centres for electronic processes in crystals. Until recently most of the quantitative studies on the cathodoplastic effect have been conducted at a “semi-microscopic scale”, e.g. by *in situ* straining experiments in a scanning electron microscope (SEM). In these experiments moving dislocations are visualized by their emergence at the sample surface, either in the cathodoluminescence mode or by the double etching technique (for a review, see [4]). Although these techniques are suitable for quantitative measurements, their poor spatial resolution makes it hardly possible to determine without ambiguity which microscopic processes of dislocation motion are affected by electronic excitation. By contrast, *in situ* straining experiments in a TEM provide a unique way to study the dislocation behaviour under electron irradiation at a microscopic scale and allow a determination of the physical parameters involved in this phenomenon. It is noteworthy that in addition to the fundamental

1
2
3
4 aspects of this research, a growing interest for such investigations is that this effect underlies
5 the degradation of optoelectronic devices: It has been recently reported that degradation and
6 ageing phenomena are associated with propagation and/or multiplication of lattice defects due
7 to carrier injection during the device operation [5-10].
8
9

10
11
12 The present paper focuses on the influence of electronic excitation on the dislocation
13 dynamics in semiconductors, at the TEM scale. A short report is given on a systematic study
14 on the radiation enhanced motion (REDM) in a single phase II-VI compound: ZnS. Thanks to
15 TEM in situ experiments the physical parameters controlling the REDM effect can be
16 identified. Then the results of an investigation of the evolution of the defect microstructure of
17 a ZnSe/GaAs epilayer under the influence of both electron beam irradiation and heating in a
18 TEM is presented. This provides information on both the strain relaxation mechanisms and
19 the degradation processes in this heterostructure.
20
21
22
23
24
25
26
27

28
29 For a better understanding of the paper, a brief summary of the properties of
30 dislocations in semiconductors will be given first.
31
32
33
34

35 **2. Properties of dislocations in semiconductors. A brief review**

36 **2.1. Dislocation mobility**

37
38
39
40
41
42
43 At low temperature dislocations with Burgers vector $1/2\langle 110 \rangle$ lie along $\langle 110 \rangle$ rows of the
44 $\{111\}$ glide planes, owing to covalent (or ionocovalent) bonding inducing a high lattice
45 friction. Therefore a glide loop consists of screw and 60° segments, that are dissociated in
46 $1/6\langle 112 \rangle$ Shockley partials (30° or 90° in character) with a stacking fault in between. In
47 compounds, due to the presence of two types of atom: A (type II or III) and B (type VI or V),
48 one has to distinguish two types of **non screw** dislocations, β and α , depending **on the position**
49 **of the extra-half plane with respect to the polar $\{111\}$ surfaces. In the medium temperature**
50 **range, dislocations are assumed to move in the so-called “glide set”: as a consequence, the**
51 **core of α dislocations contains B atoms, while the core of β ones contains A atoms [1, 2].**
52
53
54
55
56
57
58
59
60

1
2
3
4 In these crystals dislocation glide at low temperature is controlled by the Peierls
5 mechanism: A dislocation is transferred from a valley to the next one by a process consisting
6 of two elementary steps: the formation of a kink pair of critical separation and subsequent
7 kink migration along the dislocation line. At variance with metals, migrating kinks experience
8 a strong frictional force (second order Peierls relief). Dislocation glide is well described by
9 the kink diffusion model [11, 12] and can be summarized as follows. Dislocation velocities
10 have two asymptotic forms, according to whether the length (L) of the moving segment is
11 large or small as compared to the mean free path of a kink pair (X) along the dislocation line:
12
13
14
15
16
17
18
19

20 (i) for slow kink motion and/or long moving dislocation segment ($L \gg X$), the kink
21 collides and annihilates with another kink of opposite sign generated on the same segment
22 (kink collision regime). The dislocation velocity (v) is proportional to the mean free path of
23 kinks (X) and:
24
25
26
27
28
29

$$v = 2 v_D (\tau b^2 h^2 / kT) \exp\{-(F_{kp}/2 + W_m)/kT\} \quad (1)$$

30
31
32
33
34 (ii) for fast kink motion and/or short moving segment ($L \ll X$), the diffusing kink
35 reaches the end of the segment before being annihilated (kink collision-less regime). The
36 dislocation velocity is proportional to its length (L):
37
38
39
40
41
42

$$v = v_D (\tau b h^2 / kT) L \exp\{-(F_{kp} + W_m)/kT\} \quad (2)$$

43
44
45
46
47 with v_D being the trial jump frequency (equal to the Debye frequency), b the Burgers vector, h
48 the distance between adjacent Peierls valleys, τ the applied shear stress, W_m the migration
49 energy of kinks and $F_{kp}(\tau)$ the activation energy for nucleation of a kink pair.
50
51
52

53 A certain number of experimental facts led some authors to the conclusion that glide
54 of long dislocation in crystals is not in the kink collision regime. Alternatively they suggest
55 that the dislocation velocity is controlled by the presence of localized obstacles (the origin of
56 which is still debated) on the dislocation line (see [4]). In that case the mean free path of kinks
57 is the mean separation of obstacles along the dislocation line (D^*) and the dislocation velocity
58
59
60

is given by a law similar to Eq. (2) in which L is replaced by D^* . That is, the velocity is length independent, as in the kink collision regime; however, the activation energy is $F_{kp}+W_m$, as in the kink collision-less regime.

A length dependent regime of dislocation velocity has been clearly evidenced by TEM *in situ* straining experiments (for a review, see [3, 12]). In III-V compounds, the velocities of $60^\circ\beta$ and screw dislocations are proportional to their length for a given stress, up to lengths higher than a few micrometers. On the other hand a transition between the two velocity regimes has been evidenced in Si and Ge.

In the frame of the kink diffusion model, activation energies for dislocation movement can be estimated without using an Arrhenius plot. Indeed all the terms in the pre-exponential factors (equations (1) and (2)) are either known or determined experimentally. The results are summarized in Table 1.

2.2. Radiation-enhanced dislocation motion

As evidenced by experiments performed at a semi-microscopic scale, e. g. scanning electron microscopy in the cathodoluminescence mode or double etching technique, electronic excitation causes an enhancement of dislocation glide in a variety of semiconductors. The dislocation velocity can be expressed as [4]:

$$v = v_{0d}(\tau) \exp - (E_d/kT) + v_{0i}(\tau) \eta(I) \exp - (E_i/kT) \quad (3)$$

where E_d is the activation energy without excitation, i.e. electron beam intensity (I) = 0 and $E_i = E_d - \Delta E$ is the apparent activation energy under excitation; both v_{0d} and v_{0i} depend approximately linearly on the shear stress τ ; η is an efficiency factor which depends linearly on I in the low intensity range. Above a critical temperature T_c the first term dominates and no effect of excitation is observed. At lower temperatures the second term describes the dislocation motion. In Si and GaAs the main features of excitation enhanced glide do not depend on the nature of the excitation source, either electron beam or laser light [4].

1
2
3
4 The characterization of the microscopic processes affected by excitation requires
5 which condition of dislocation velocity (length dependent or length independent) is actually
6 realized in the experiments performed at a semi-microscopic scale. As described below *in situ*
7 deformation experiments in a TEM give further information on the behaviour of dislocations
8 under excitation at a microscopic scale.
9
10
11
12
13
14

15 16 17 **3. Electron beam irradiation enhanced dislocation motion in ZnS [13, 14]**

18
19
20 The effect of electron beam excitation on the dislocation behaviour in cubic (sphalerite) ZnS
21 single crystals has been studied in the temperature range room temperature-500 K. During *in*
22 *situ* straining experiments (foil surface (011); tensile axis $[2\bar{1}1]$) the dislocation motion is
23 observed to be very smooth and viscous, whatever the temperature and the electron beam
24 intensity (in the range 35-5600 A/m²). This strongly suggests that the dislocation glide is still
25 controlled by the Peierls mechanism, even in the enhancement regime. Dislocation sources
26 are frequently observed: In the example shown in figure 1 the single-ended source rotates
27 counter-clockwise, the screw direction being almost parallel to the slip traces. Dislocation
28 segments lie along the $\langle 110 \rangle$ rows of the $\{111\}$ slip plane.
29
30
31
32
33
34
35
36
37
38

39 In all the studied temperature range and electron beam intensity range the dislocation
40 velocity varies linearly with its length [13, 14]. This suggests that no kink collision takes
41 place before the initial kink pair reaches the ends of the moving segment (kink collision-less
42 regime). As indicated above a strong enhancement of dislocation mobility under electronic
43 excitation is evidenced. Figure 2 reports an example of the variation of $P = v/L$ with I . At low
44 intensity P varies linearly with I , in agreement with the law deduced from experiments
45 performed at a semi-microscopic scale (equation (3)). The extrapolation of the curve to $I = 0$
46 gives an estimate of the dislocation mobility in the absence of electron beam excitation, from
47 which the data reported on Table 1 for this compound are determined. As I increases, the
48 curves $P(I)$ deviate from a linear relationship and P seems to come to a saturation level for
49 electron beam intensities higher than about 1500 A/m².
50
51
52
53
54
55
56
57
58
59
60

1
2
3
4 As the parameter η in equation (3) is not known the determination of activation
5 energies under electronic excitation requires the use of an Arrhenius plot: it is found $E_i = 0.3$
6 ± 0.1 eV, to be compared with the activation energy in the absence of electronic excitation: E_d
7 $= 1.15 \pm 0.1$ eV; that is $\Delta E/E_d$ is as high as 75% in this compound [14].

8
9
10
11
12 The observed excitation-enhanced dislocation glide is interpreted in terms of the
13 reduction of activation energy by non radiative recombination of injected carriers at electronic
14 levels associated with dislocations. There are two elementary steps of dislocation motion that
15 could be assisted by the lattice vibrations induced by these multiphonon processes: the kink
16 pair formation and the kink migration. The theoretical analysis [4] showed that in the kink-
17 collision less regime, the linear dependence of the dislocation velocity with electron beam
18 intensity (at low injection level) is a proof that kink pair formation is enhanced; kink
19 migration, even if it occurs, does not contribute to the reduction in activation energy. This
20 reduction in activation energy is therefore interpreted as the difference between an electronic
21 energy level associated with a straight portion of dislocation and a relevant band edge.

22
23
24
25
26
27
28
29
30
31
32
33 The tendency to saturation of P at high electron beam intensities can be explained by
34 the expected saturation of the recombination rate at high generation rates of electron-hole
35 pairs; that is in the high intensity regime, the dislocation velocity depends only weakly on the
36 beam intensity.

37
38
39
40
41 In this material, deformation proceeds mainly by glide of perfect dislocations. Owing
42 to the low stacking fault energy (< 6 mJ/m²), glide of uncorrelated partial dislocations is
43 occasionally observed; it is noteworthy that the observed dynamic behaviour of these defects
44 under electronic excitation is very similar to that of perfect dislocations [15].

4. Defect dynamics in a ZnSe/GaAs heterostructure

45
46
47
48
49
50
51
52
53
54
55
56
57
58
59
60
Electron excitation also affects the defect behaviour in semiconducting heterostructures. We
report here on the results of *in situ* heating experiments performed on a ZnSe epilayer grown
on a GaAs substrate, which could be considered as a prototype structure for devices emitting
in the blue region of the optical spectrum. One of the main obstacles in the development of

1
2
3
4 reliable light emitters based on II-VI semiconductor heterostructures is their short operation
5
6 time. The degradation of their optical properties is attributed to the presence of structural
7
8 defects and to their multiplication under the operation conditions: stacking faults and/or
9
10 dislocations acting as sources of new defects activated by REDM. It has been shown recently
11
12 [16] that the simultaneous influence of electron beam irradiation and specimen heating (above
13
14 420K) leads to the degradation of the active layer by nucleation and propagation of structural
15
16 defects, associated with a climb mechanism. Dislocation multiplication is strongly activated
17
18 by the electron beam; indeed, when the electron beam is off, the microstructure is not
19
20 modified by annealing in the studied temperature range. Thus the climb mechanisms involved
21
22 in the degradation process are assisted by the non-radiative recombination of electron hole
23
24 pairs created by the electron beam.
25

26
27 We focus here on the behaviour of as-grown defects, in connection with the strain
28
29 relaxation mechanisms in this material.
30

31 32 33 **4.1. Experimental details**

34
35
36
37 Samples are (001) ZnSe/GaAs heterostructures grown by Molecular Beam Epitaxy (MBE) at
38
39 280°C at the Centre de Recherche sur l'Hetero-Epitaxie et ses Applications (CRHEA),
40
41 Valbonne (France), with an excess of Se [17]. The layer is 250 nm thick, larger than the
42
43 critical thickness (130nm). However, X-ray diffraction experiments reveal that the ZnSe layer
44
45 is not fully relaxed [18] (see also below). The lattice parameter of ZnSe is slightly larger than
46
47 that of GaAs, so that the layer is in compression (misfit 0.27%) Comparing the thermal
48
49 expansion coefficients of ZnSe and GaAs indicates that the misfit compression increases
50
51 during heat treatment. TEM plan-view specimens are prepared by chemical etching of GaAs
52
53 substrate and subsequent ion milling from the back side until perforation [18].
54

55
56 Conventional TEM and *in situ* heating experiments (in the range room temperature-
57
58 570 K) are done in a JEOL 2010 FX TEM, operated at 200kV. In these experiments, the
59
60 electron beam intensity is varied by changing the excitation of the condenser lens. Large angle

1
2
3
4 convergent beam electron diffraction (LACBED) experiments are done in a Philips CM30
5
6 TEM.

7
8 As the sphalerite structure is non-centrosymmetric, the absolute polarity of the sample
9
10 has to be determined. In the course of this study a novel method has been used: CBED on
11
12 {001} plan view samples [19].
13

14 15 16 **4.2. The as-grown defect microstructure in the ZnSe layer** 17

18
19 A large variety of defects are observed in the ZnSe/GaAs heterostructures, depending on the
20
21 growth conditions, the initial treatment of the growth surface, the doping of the ZnSe layer,
22
23 etc... The defects present in our samples are described below: they are **predominantly**
24
25 undissociated misfit dislocations and stacking faults.
26
27

28
29
30
31 **4.2.1. Misfit dislocations.** An array of misfit dislocations is present in the material (figure 3).
32
33 **Their Burgers vector $1/2\langle 011 \rangle$ is inclined to the interface.** Few are along $\langle 110 \rangle$ directions
34
35 (marked B on the figure); most of them lie along unusual $\langle 310 \rangle$ directions (marked A) and
36
37 **show slight undulations. Taking into account the efficient Burgers vector component (i.e. the**
38
39 **component of the Burgers vector in the interface plane, perpendicular to the misfit dislocation**
40
41 **line) dislocations A are more efficient to relax the misfit strain than dislocations B[‡].** It was
42
43 recently shown that the early stages of stress relaxation in this heterostructure proceeds by
44
45 activation of secondary $1/2\langle 011 \rangle\{133\}$ slip systems [20]. **From the efficient Burgers vector**
46
47 **component** and the mean distance between interfacial dislocations, the misfit strain that is
48
49 released by this network is estimated as 6×10^{-4} , to be compared to the crystallographic misfit:
50
51 27×10^{-4} . This is another indication that the layer is not completely relaxed.
52
53

54
55
56 **4.2.2. Isolated triangular “stacking faults”.** Figure 4 shows an example of this defect,
57
58 which are randomly distributed in the layer. They look like triangular stacking faults, the
59

60

[‡] Since the Burgers vector of dislocations A is inclined to the interface, these are not the most efficient strain-releasing misfit dislocations. Dislocations lying along $\langle 110 \rangle$ directions within the interface plane and with in-plane $1/2\langle 110 \rangle$ Burgers vector are most efficient (see § 4.3.5)

1
2
3
4 apex of the triangle being located close to the interface; it is noteworthy that they are present
5
6 only in two {111} planes with the same polarity: (111) and ($\bar{1}\bar{1}1$). Their TEM diffraction
7
8 contrast is similar to that of an extrinsic stacking fault (figure 4(b)). The bounding dislocations
9
10 are straight. One partial is of Shockley type, as determined by contrast analysis [18], but we
11
12 failed to determine the exact nature of the second partial. Nevertheless it is not of Frank type.
13
14 In this material a high resolution TEM investigation of defects exhibiting such an extrinsic
15
16 stacking fault contrast in strong beam conditions showed that they were extrinsic-intrinsic
17
18 fault pairs at a spacing 7-10 nm [21]. Consistent with this result we do not observe line
19
20 splitting in the LACBED patterns of the defect (figure 4(c)), suggesting that the net fault
21
22 vector is a lattice translation, as it is expected from an intrinsic-extrinsic fault pair. Under
23
24 electron excitation (see below), it is observed that the Shockley partial is glissile. This is not
25
26 consistent with the defect being a stacking fault trapezoid limited by stair rods as described by
27
28 Fung *et al.* [22]. Further work is needed to understand the crystallographic nature of this
29
30 defect.
31
32
33
34

35 **4.2.3. Paired triangular stacking faults** (figure 5). These defects, which look like a bow tie,
36
37 are oppositely oriented stacking faults bound by Shockley partials, the apex of the triangle
38
39 being close to the interface. Diffraction contrast experiments, as well as LACBED
40
41 experiments indicate that all the stacking faults are intrinsic. The stacking faults lie either in
42
43 the two {111} planes in the [110] zone, or in the two {111} planes in the $\bar{1}\bar{1}0$ zone; both
44
45 configurations are equally observed, indicating that there is no polarity effect in this particular
46
47 configuration. Similar defects have been observed in ZnSe-based heterostructures [9, 23].
48
49 This configuration is suggested to result from the dissociation of a prismatic half-loop of
50
51 Burgers vector $1/2\langle 110 \rangle$ (in the interface plane) in two {111} planes in the Burgers vector
52
53 zone, according to the reactions (written here for a dislocation with Burgers vector $1/2[1\bar{1}0]$):
54

55 - in the (111) plane: $1/2[1\bar{1}0] \rightarrow 1/6[2\bar{1}\bar{1}] + 1/6[1\bar{2}1]$

56
57 - in the ($\bar{1}\bar{1}1$) plane: $1/2[1\bar{1}0] \rightarrow 1/6[2\bar{1}1] + 1/6[1\bar{2}\bar{1}]$

58
59 Note that the total prismatic dislocation is edge in character.
60

1
2
3
4 The stacking faults are observed to be widened in the vicinity of the sample surface.
5
6 This is accounted for by considering the force acting on each partial, due to the misfit stress.
7
8 Indeed, calculations indicate that the glide components are orientated in such a way that they
9
10 lead to a widening of the stacking fault ribbon in each plane (note that there is no force acting
11
12 on the total dislocation). This widening effect could be enhanced by the contribution of image
13
14 forces. Note that this results in an increase of the dislocation lengths. In thicker layers, this
15
16 stress effect is certainly balanced by the increase of the line energy of the Shockley partials
17
18 and a narrowing of the fault ribbon is observed [23].
19
20
21

22
23 **4.2.4. Concluding remarks.** It is noteworthy that no Frank stacking faults are present in our
24
25 samples [18]. This is at variance with the results of the literature on both single triangular
26
27 faults [9, 23] and paired stacking faults [24]. This is certainly related to the growth conditions
28
29 of the ZnSe layer [25-27].
30
31
32

33 **4.3. Evolution of the defect microstructure during TEM in situ heating experiments.**
34
35 **Observations and discussion.**
36
37

38 The defect microstructure in the ZnSe layer changes during TEM observations. Indeed, as
39
40 detailed below, the as-grown stacking faults may transform into new defects, because of
41
42 dislocation movements, activated by the temperature increase and/or the electron excitation.
43
44 In addition, new defects are generated, which contribute to strain relaxation in the ZnSe layer.
45
46 Finally, as indicated above, a complete degradation of the layer is observed. Before going into
47
48 details, an important point has to be stressed. No alteration of the layer microstructure is
49
50 observed after a several hours of annealing the sample in the heating stage of the holder at a
51
52 temperature as high as 520 K, while the electron beam is off. That means that the below-
53
54 described events are not only thermally activated (they are enhanced by a temperature
55
56 increase), but also affected by the electronic excitation.
57
58

59 **4.3.1. Misfit dislocations.** These dislocations play a role in the degradation process. Above
60
420 K, small perfect dislocation loops nucleate on pre-existing interfacial dislocations by

point defect accumulation consistent with a radiation enhanced climb mechanism. This has been described in another paper [16] and will not be discussed further here.

4.3.2. Triangular stacking faults. Even if the exact nature of this defect is not completely understood, one of the bounding dislocations is identified as a Shockley partial. Under electron excitation this partial is mobile and moves towards the second (immobile) dislocation and the stacking fault in between is eliminated. This is illustrated on figure 6, which shows three pictures taken from a video recording. It is seen that in a first step the mobile partial bends in the stacking fault plane and finally recombines with the second dislocation. Note that the surface acts as a pinning site. That process (complete elimination of the fault) takes 24 seconds at room temperature and only 3 seconds at 373 K; that is the dislocation movement is thermally activated.

From this experiment, one can estimate the activation energy for dislocation motion under electron excitation. TEM *in situ* straining experiments in single phase ZnSe crystals [28] have demonstrated that the dislocation mobility is independent of the electron beam intensity for $I \geq 1000 \text{ A/m}^2$, which is the intensity level in our experiments on the ZnSe/GaAs structure, that is η (equation (3)) could be considered as a constant. Moreover, the length of the mobile dislocation is fixed by the thickness of the ZnSe layer, which is constant in all experiments (250 nm), so that we are not concerned with a possible length effect on dislocation velocity. Finally the pre-exponential factor in the expression for dislocation velocity (equation (3)) depends linearly on the shear stress τ . Then, considering two experiments performed at temperatures $T_1 = \text{room temperature}$ and $T_2 = 373 \text{ K}$, labelled (1) and (2), respectively, one has:

$$E_i = k \frac{T_1 T_2}{T_2 - T_1} \ln \frac{\tau_1 v_2}{\tau_2 v_1} \quad (4)$$

The shear stress ratio is proportional to the misfit stress ratio, so it is proportional to the misfit parameter (f); we assume that the dislocation velocity is inversely proportional to the recombination time (t). We end up with:

$$E_i = k \frac{T_1 T_2}{T_2 - T_1} \ln \frac{f_1 t_1}{f_2 t_2} \quad (5)$$

1
2
3
4 With $f_1 = 0.27\%$, $f_2 = 0.29\%$ (calculated from the variations of the thermal expansion
5 coefficients of GaAs and ZnSe) and $t_1 = 24\text{s}$, $t_2 = 3\text{s}$, as determined from *in situ* experiments,
6 we estimate $E_i = 0.25\text{ eV}$. The comparison with the activation energy in the absence of
7 electron excitation is not straightforward: indeed experimental data on Shockley partials are
8 still lacking. However the activation energy for perfect dislocation glide in the absence of
9 electron excitation has been estimated in single phase ZnSe crystals: $E_d = 0.7 \pm 0.1\text{ eV}$ [29][§]. It
10 has been shown that in the parent compound ZnS, the activation energies for both partial and
11 perfect dislocations are very similar [15]. If we assume that this is also the case for ZnSe, then
12 we can take this as another evidence of a REDM effect in this compound.
13
14
15
16
17
18
19
20
21
22
23
24

25 Finally, it should be noticed that the dislocation mechanism described here does not
26 play a role in the strain relaxation mechanisms, since no dislocations are generated at the
27 interface.
28
29
30
31
32

33 **4.3.3. Paired stacking faults.** This particular defect configuration acts as a source for
34 heterogeneous nucleation of screw misfit dislocations in the interface. This is illustrated on
35 figure 7, which is taken from a video recording ($T = 373\text{ K}$). It is seen that the two partials
36 bounding one of the two stacking faults recombine in a perfect dislocation of edge character.
37 Then this perfect dislocation glides and bows out in its own $\{111\}$ glide plane (note again that
38 the surface acts as a pinning site). After the dislocation has escaped from its surface pinning
39 point it moves very rapidly, leaving a screw dislocation in the interface. A similar mechanism
40 is observed to occur on the second stacking fault of the pair. At this temperature the
41 “recombination and unpinning” sequence takes 7 min; in contrast the dislocation glide is very
42 rapid since screw dislocations of lengths longer than $10\text{ }\mu\text{m}$ are formed in less than 10 s. A
43 similar mechanism has already been reported in $\text{ZnS}_x\text{Se}_{1-x}/\text{GaAs}$ heterostructures (x around
44 0.05) [9]. In that case the active layer was about 450 nm thick, and the stacking fault ribbons
45 are very narrow (see § 4.2.3. above). Then the recombination phase is probably easier in this
46
47
48
49
50
51
52
53
54
55
56
57
58
59
60

[§] This value is in good agreement with the results of a recent investigation on the strength of ZnSe by means of compressive deformation, where the activation energy for dislocation motion was estimated to be 0.5-0.7eV[30]

1
2
3
4 material. Another transformation of these paired stacking faults leading to the formation of
5 Frank stacking faults has been observed in 70 nm thick $\text{ZnS}_{0.04}\text{Se}_{0.94}$ [31]. It is suggested that
6 in this case, the mechanism described above is not operative, because the recombination of
7 the partials is too difficult.
8
9

10
11
12 The driving force for the formation of this network of screw dislocations is not
13 completely understood. First, as indicated above, the net glide force acting on the total
14 (recombined) dislocation due to the misfit stress is zero; nevertheless the dislocation bows out
15 in its slip plane. Second, an arrangement of screw dislocations at the interface does not release
16 the misfit stress, unless some shear stress is present. We have to admit that some stress
17 inhomogeneities are present in our samples. These stress inhomogeneities could be due either
18 to stacking errors during the growth process or to the thinning process, which could induce a
19 loss of the local fourfold symmetry of the (001) sample.
20
21
22
23
24
25
26
27
28
29
30

31 **4.3.4. Formation and extension of extrinsic stacking faults bounded by Shockley partial**
32 **dislocations.** Half-loops of Shockley partial dislocations bounding an extrinsic stacking fault
33 are nucleated at the sample surface during the TEM observation (figure 8). The extrinsic
34 nature of the fault, as well as the Burgers vector of the bounding partial have been determined
35 from diffraction contrast experiments in dynamical 2-beam conditions, as well as from
36 LACBED experiments [18]. Like the isolated triangular stacking faults (§ 4.2.2), they are
37 formed only in the {111} planes belonging to the $[\bar{1}10]$ zone: (111) and $(\bar{1}\bar{1}1)$, which have the
38 same polarity. The Burgers vector of the Shockley partial is perpendicular to $[\bar{1}10]$.
39
40
41
42
43
44
45
46

47 The nucleation site is some heterogeneity at the sample surface. In the first stage, the
48 defect size is very short. Further annealing at temperatures higher than 373 K causes the
49 expansion of the loop in the fault plane, leading to the formation of a wide stacking fault (a
50 few micrometer wide, figure 8). At the interface, the Shockley partial is edge in character. The
51 dislocation movement is smooth and regular (viscous glide), indicating that it is subjected to
52 lattice friction. At 373 K, an estimate of the velocity of the threading segments is 40 ± 10
53 nm/s, of the same order of magnitude as the velocity of the Shockley partials bounding the
54 isolated triangular faults.
55
56
57
58
59
60

1
2
3
4 The sense of dislocation movement is consistent with the sense of the force due to the
5 misfit stress. Equivalently, the efficient Burgers vector component ($1/6\langle 110 \rangle$) is consistent
6 with a slight plastic relaxation of the misfit strain.
7
8

9
10 Only extrinsic stacking faults present a polarity effect. Although, **previously,**
11 **investigators do** not seem to **have paid** attention to this, examination of the literature [9, 23,
12 27, 32] indicates that there is a systematic correlation between the extrinsic nature of the
13 stacking fault and the polarity of the sample, even when the observed configurations are
14 different **from** those observed in our samples.
15
16

17
18 In the present study, we suggest that this polarity effect is related to the chemical
19 nature of the atomic row in the dislocation core. **Modelling of the dislocation core indicates**
20 **that** partials **bounding an extrinsic stacking fault**, nucleated at the sample surface and moving
21 towards the interface in $\{111\}$ planes **belonging to the** $[\bar{1}10]$ **zone** have Se atoms in their core;
22 “efficient” partials moving in the two other $\{111\}$ planes would have Zn atoms in their core.
23 (These dislocations are labelled Se- and Zn-dislocations, respectively)*. Then we conclude
24 that nucleation and propagation of Se-dislocations is easier than nucleation and propagation of
25 Zn-dislocations **also**. This is consistent with an earlier investigation of dislocation mobility in
26 bulk ZnSe by etch pit experiments. Indeed Kirichenko *et al.* [33] have shown that the mobility
27 of perfect Se-dislocations (**i.e. of α type**) is more than 100 times higher than that of perfect
28 Zn-dislocations (**β type**). This large asymmetry is certainly valid for partial dislocations.
29
30
31
32
33
34
35
36
37
38
39
40
41
42
43
44

45 **4.3.5. Complete relaxation of the ZnSe layer by formation of a network of edge**
46 **dislocations (figure 9).** Heating the sample up to 523 K under electron beam causes the
47 sudden formation of a cross grid of perfect edge dislocations with $1/2\langle 110 \rangle$ Burgers vectors
48 in the interface (figure 9(a)). These dislocations are very efficient to completely relax both the
49 misfit stress and the thermal stress. The formation of this array is very fast so that the
50 generation mechanism could not be detailed: it is observed (figure 9(b)) that new misfit
51 dislocations are formed at the interface during only one video frame (frame duration 1/50 s).
52
53
54
55
56
57
58
59
60

** The labelling α or β could be confusing in the case of Shockley partials bounding an extrinsic stacking fault: indeed these partials could be regarded as composite partials moving on two adjacent planes.

1
2
3
4 Again it should be stressed that these events **are** greatly enhanced by electron excitation since
5
6 annealing of the sample “in the dark” did not lead to a noticeable modification of the defect
7
8 microstructure at the ZnSe/GaAs interface.
9

10 11 12 **5. Conclusion.** 13

14
15
16 Since the pioneering work of Hirsch *et al.* [34], who were the first to report dislocation
17
18 movements under thermal stresses generated by the electron beam, our knowledge of the
19
20 **dislocation dynamics** under various excitations has been tremendously improved. In this paper
21
22 we have focused on the effect of electronic excitation on the properties of dislocations in
23
24 semiconducting materials. In ZnS, the elementary dislocation mechanisms that are affected by
25
26 non radiative recombination of charge carriers have been identified, thanks to TEM *in situ*
27
28 straining experiments at different temperatures and different electron beam intensities. In
29
30 ZnSe/GaAs heterostructures, a complex defect microstructure is present in as-grown samples.
31
32 Heating the sample under electron irradiation induces a variety of dislocation behaviours,
33
34 some of them being related to misfit strain relaxation. Again dislocation movements are
35
36 enhanced by electron excitation. TEM *in situ* **also** experiments provide a useful tool to study
37
38 the degradation processes in this compound **in real time**.
39
40
41
42
43
44
45
46
47
48
49
50
51
52
53
54
55
56
57
58
59
60

Références

- [1] H. Alexander, in *Dislocations in Solids*, Vol. 7, edited by F.R.N. Nabarro (Elsevier, Amsterdam, 1986) pp. 113-234
- [2] A. George and J. Rabier, *Revue Phys. Appl.* **22** 941 (1987)
- [3] G. Vanderschaeve, C. Levade and D. Caillard, *J. Microsc.* **203** 72 (2001)
- [4] K. Maeda and S. Takeuchi, in *Dislocations in Solids*, Vol.10, edited by F.R.N. Nabarro and M.S. Duesbery (Elsevier, Amsterdam, 1996) pp. 443-504
- [5] B.C. De Cooman, C.W.T. Bulle-Lieuwma, J.A. De Poorter, *et al.*, *J. Appl. Phys.* **67** 3919 (1990)
- [6] K. Maeda, Y. Yamashita, N. Maeda, *et al.*, *Mat. Res. Soc. Proc.* **184** 69 (1990)
- [7] S. Guha, J.M. De Puydt, J. Quiu, *et al.*, *Appl. Phys. Lett.* **63** 3023 (1993)
- [8] M. Hovinen, J. Ding, A. Salokatve, *et al.*, *J. Appl. Phys.* **77** 4150 (1995)
- [9] L.H. Kuo, L. Salamanca-Riba, B. Wu, *et al.*, *J. Vac. Sci. Technol. B* **13** 1694 (1995)
- [10] J.M. Bonard, J.D. Ganière, L. Vanzetti, *et al.*, *J. Appl. Phys.* **84** 1263 (1998)
- [11] J.P. Hirth and J. Lothe, *Theory of Dislocations* (McGraw-Hill, New York, 1968) pp. 484-496
- [12] D. Caillard, J.L. Martin, *Thermally Activated Mechanisms in Crystal Plasticity* (Pergamon, Amsterdam, 2003) pp. 229-241
- [13] A. Faress, C. Levade and G. Vanderschaeve, *Phil. Mag. A* **68** 97 (1993)
- [14] C. Levade, A. Faress and G. Vanderschaeve, *Phil. Mag. A* **69** 855 (1994)
- [15] A. Faress, S. Farenc, C. Levade, *et al.*, *Phys. Stat. Sol. (a)* **137** 435 (1993)
- [16] S. Lavagne, C. Levade and G. Vanderschaeve, *Mat. Sci. Eng. B* in press
- [17] V. Bousquet, E. Tournié and J.P. Faurie, *J. Cryst. Growth* **192** 102 (1998)
- [18] S. Lavagne, Ph. D. Thesis n° 659 INSA Toulouse (2002)
- [19] S. Lavagne, C. Roucau, C. Levade, *et al.*, *Phil. Mag. A* **82**, 1451 (2002)
- [20] S. Lavagne, C. Levade and G. Vanderschaeve, *J. Phys.: Condens. Matter* **14** 13291 (2002)
- [21] C. Y. Chen, W. M. Stobbs and E. G. Bithell, *Phil. Mag. A* **72**, 1173 (1995)

- 1
2
3
4 [22] K. K. Fung, N. Wang and I. K. Sou, Appl. Phys. Lett. **71**, 1225 (1997)
5
6 [23] J.M. Bonard, J.D. Ganière, S. Heun, *et al.*, Phil. Mag Letters **75**, 219 (1997)
7
8 [24] J. Petruzello, D.A. Greenberg, A. Cammak, *et al.*, J. Appl. Phys. **63**, 2299 (1988)
9
10 [25] A. Rosenauer, T. Reisinger, F. Franzen *et al.*, J. Appl. Phys. **79**, 4124 (1996)
11
12 [26] L.H. Kuo, K. Kimura, S. Miwa *et al.*, Appl. Surf. Sci. **117-118**, 495 (1997)
13
14 [27] S. Heun, J. J. Pagel, L. Sobra *et al.*, Appl. Phys. Lett. **70**, 237 (1997)
15
16 [28] C. Levade and G. Vanderschaeve, J. Cryst. Growth **197**, 565 (1997)
17
18 [29] C. Levade, G. Vanderschaeve, G.Rivaud *et al.*, in *Electron Microscopy 1994*, Vol. 2A,
19 edited by B. Jouffrey, C. Colliex, J. P. Chevalier, F. Glas and P. W. Hawkes (les Editions de
20 Physique, Paris, 1994) pp. 67-68
21
22 [30] I. Yonenaga, K. Watanabe, S. Itoh *et al.*, *Physica B* **376-377**, 771 (2006)
23
24
25 [31] D. Litvinov, A. Rosenauer and D. Ghertsens, Phil. Mag. Letters **83**, 575 (2003)
26
27 [32] J. Tanimura, O. Wada, T. Ogama *et al.*, J. Appl. Phys. **77**, 6223 (1995)
28
29 [33] L.G. Kirichenko, V.F. Petrenko and G. V. Ulmin, Soviet Phys. JETP **47**, 289 (1978)
30
31 [34] P.B. Hirsch, J.W. Horne and M. J. Whelan, Phil. Mag. **1**, 677 (1956)
32
33
34
35
36
37
38
39
40
41
42
43
44
45
46
47
48
49
50
51
52
53
54
55
56
57
58
59
60

1
2
3
4 **Tables**
5
6
7

8 Table 1. Activation parameters for dislocation glide as estimated from TEM *in situ*
9 straining experiments. Experimental data are analysed in the frame of the kink diffusion
10 model
11
12
13

material	dislocation	temperature (K)	stress (MPa)	X (μm)	$F_{kp}(\tau)$ (eV)	W_m (eV)	F_k (eV)
Si	60°, screw	793-888	240		1.2	1.3	0.9
Si	60°, screw	813	550	0.4	0.9	1.3	0.9
Ge	60°	703	40	0.55	0.8	0.85	0.5
Ge	screw	678	35	0.7	0.8	0.9	0.5
InSb	screw, 60° β	523	50	> 5	0.8-1.2	< 0.4	0.5-0.65
InP	screw, 60° β	623	50	> 0.7	0.8-1.5	< 0.7	
GaAs	screw, 60° β	623	50	> 3	1.1-1.6	< 0.5	0.65-0.9
ZnS	60°, screw	473	25-40	> 0.4	0.85-1.15	< 0.3	0.5-0.65

14
15
16
17
18
19
20
21
22
23
24
25
26
27
28
29
30
31
32
33
34
35
36
37
38
39
40
41
42
43
44
45
46
47
48
49
50
51
52
53
54
55
56
57
58
59
60

Figures Captions

Figure 1: Dislocation source in ZnS: slip system $1/2[0\bar{1}1](111)$. $T = 293$ K; $I = 5600$ A/m²; $\tau = 40 \pm 10$ MPa.

Figure 2: The velocity per unit length vs. electron beam intensity in ZnS. Room temperature; $\tau = 25 \pm 5$ MPa.

Figure 3: Misfit dislocations at the ZnSe/GaAs interface; their Burgers vector is inclined to the interface: (A): dislocations along $\langle 310 \rangle$; (B) dislocations along $\langle 110 \rangle$; (T) threading dislocation.

Figure 4: (a) Three isolated triangular stacking faults, randomly distributed in the ZnSe layer, bright field, $\mathbf{g} = (220)$; (b) Dark field image ($\mathbf{g} = (220)$) showing the extrinsic-like contrast of the stacking fault: the opposite of the diffraction vector points towards a dark fringe; (c) LACBED pattern (the stacking fault appears as a shadow image): there is no shift of the diffraction lines.

Figure 5: Paired stacking faults (a) Bright field image; (b) Schematics of the two possible configurations as observed in (001) projection; (c) Schematics of the observed configuration, which can be regarded as a prismatic half loop dissociated in two secant planes.

Figure 6: Electron excitation induced elimination of a triangular stacking fault by glide of the bounding Shockley partial, room temperature (a) $t = 0$ s; (b) $t = 8$ s; (c) $t = 24$ s.

Figure 7: Electron excitation induced evolution of a paired stacking faults, $T = 373$ K (a) $t = 0$ s; (b) $t = 420$ s the two partials have recombined and the perfect dislocation bows out in its slip plane; (c) $t = 440$ s the dislocation movement leaves a screw dislocation at the interface; (d) $t = 960$ s a similar transformation is achieved on the second stacking fault of the pair.

1
2
3
4 Figure 8: Half loops of Shockley partials limiting an extrinsic stacking fault, $T = 373 \text{ K}$ (a)
5 Just after the nucleation stage; (b) One of the half loops expands in its plane to reach the
6 interface
7
8
9

10
11
12 Figure 9 $T = 523 \text{ K}$ (a) Formation of a cross grid of edge dislocations which completely relax
13 the misfit strain; (b) Two **micrographs** taken 10 s apart: each of the newly formed
14 dislocations (arrowed) appeared during a video frame duration (1/50s); one family is out of
15 contrast
16
17
18
19
20
21
22
23
24
25
26
27
28
29
30
31
32
33
34
35
36
37
38
39
40
41
42
43
44
45
46
47
48
49
50
51
52
53
54
55
56
57
58
59
60

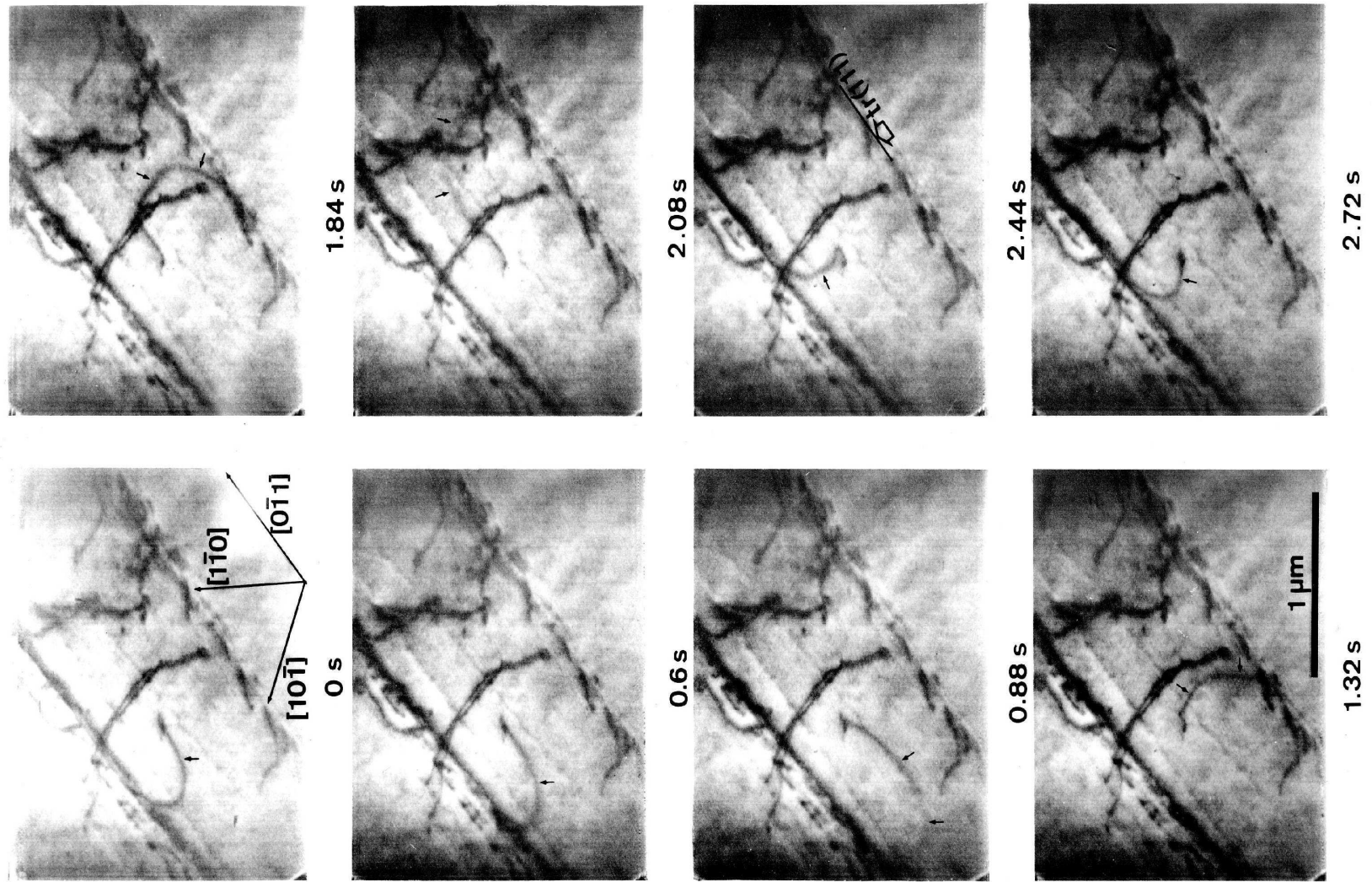


Figure 1

1
2
3
4
5
6
7
8
9
10
11
12
13
14
15
16
17
18
19
20
21
22
23
24
25
26
27
28
29
30
31
32
33
34
35
36
37
38
39
40
41
42
43
44
45
46
47
48
49

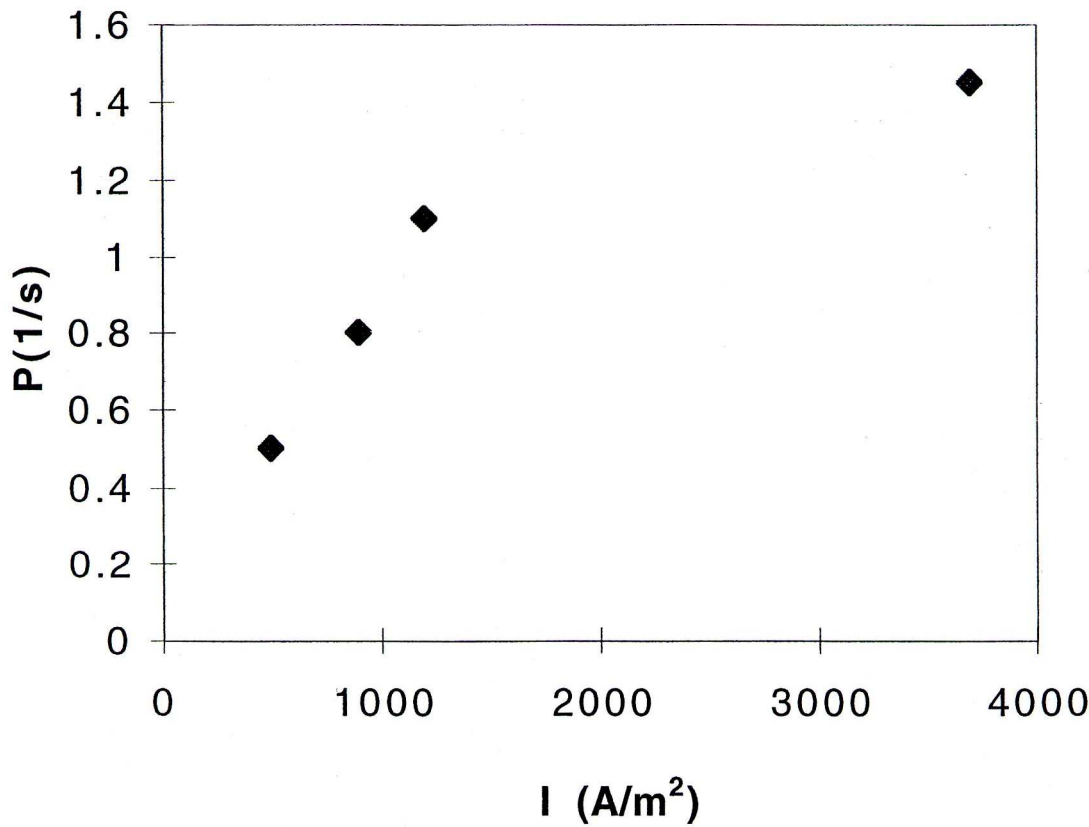


Figure 2

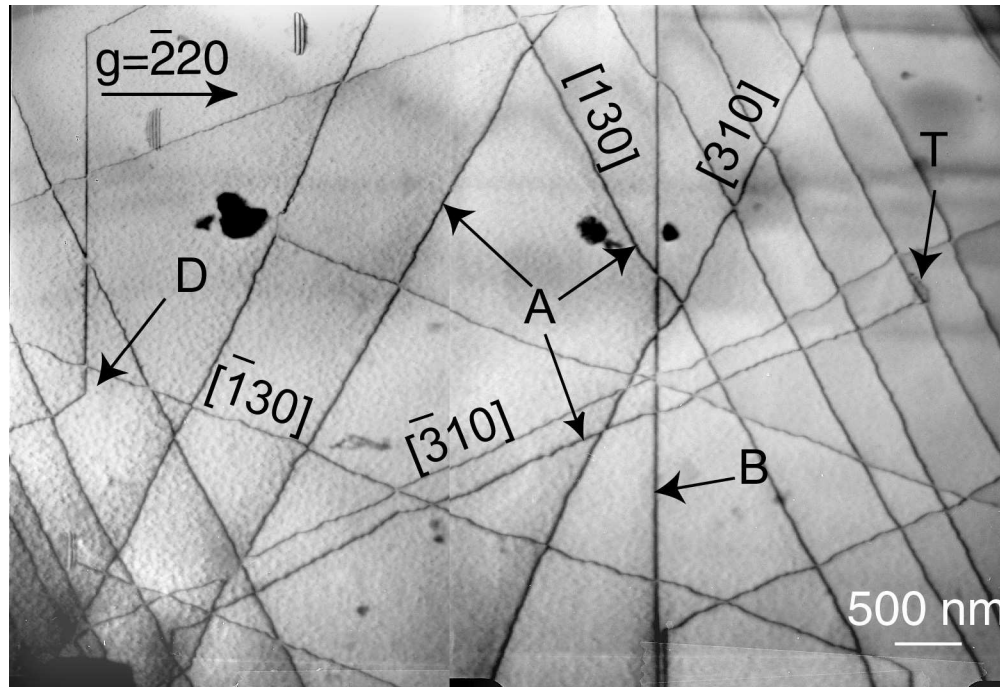


Figure 3

1
2
3
4
5
6
7
8
9
10
11
12
13
14
15
16
17
18
19
20
21
22
23
24
25
26
27
28
29
30
31
32
33
34
35
36
37
38
39
40
41
42
43
44
45
46
47
48
49

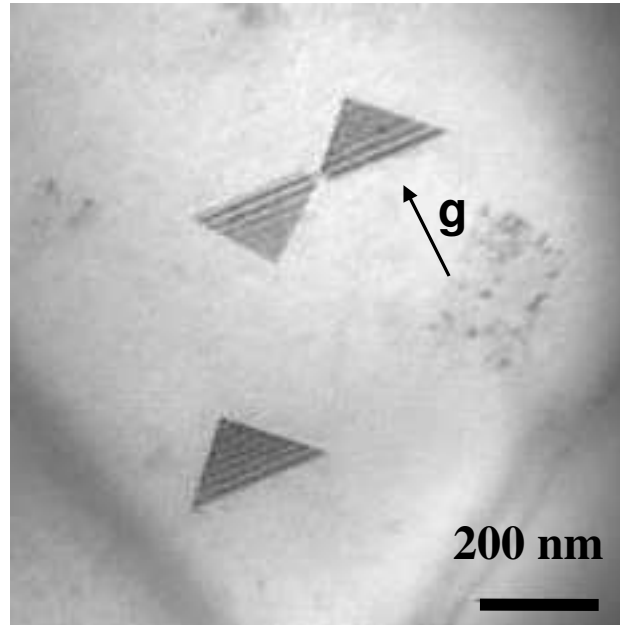


figure 4a

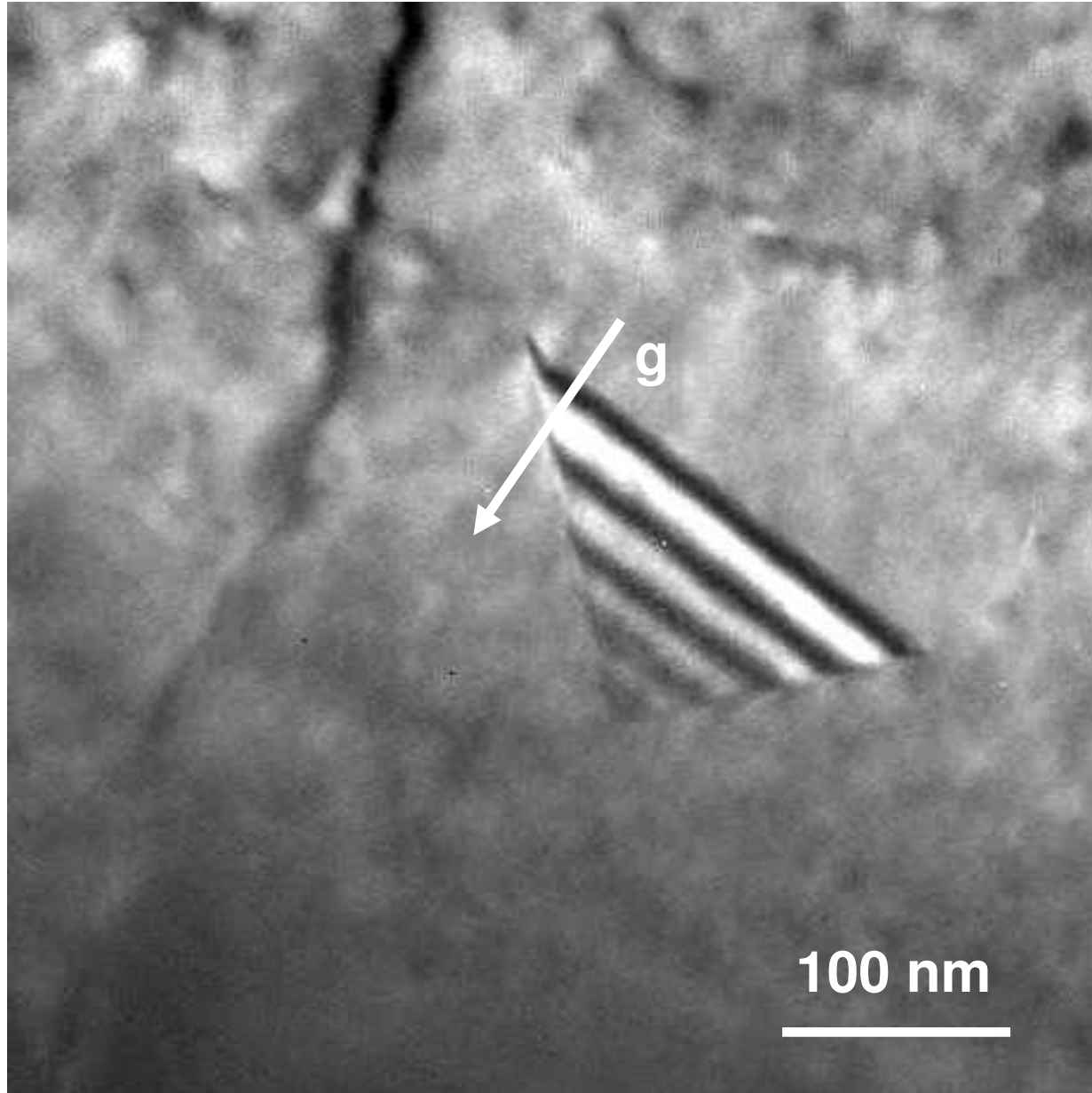


figure 4b

1
2
3
4
5
6
7
8
9
10
11
12
13
14
15
16
17
18
19
20
21
22
23
24
25
26
27
28
29
30
31
32
33
34
35
36
37
38
39
40
41
42
43
44
45
46
47
48
49

1
2
3
4
5
6
7
8
9
10
11
12
13
14
15
16
17
18
19
20
21
22
23
24
25
26
27
28
29
30
31
32
33
34
35
36
37
38
39
40
41
42
43
44
45
46
47
48
49

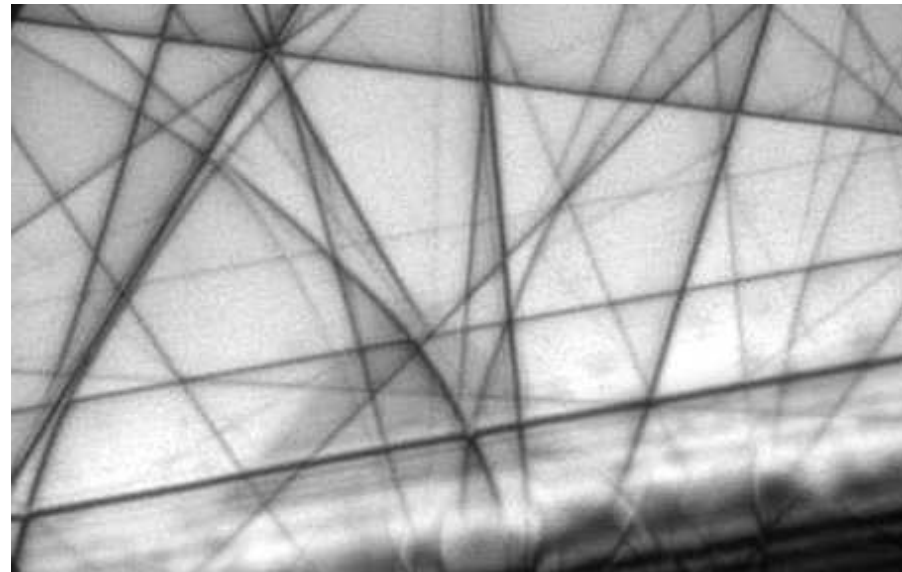
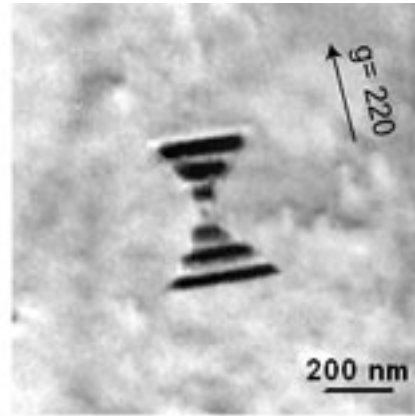
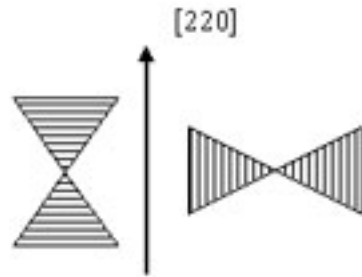


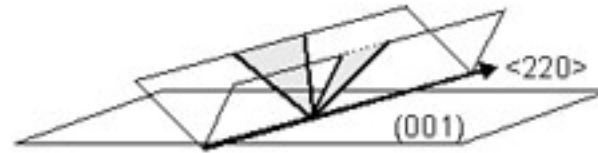
Figure 4c



-a-



-b-



-c-

Figure 5

1
2
3
4
5
6
7
8
9
10
11
12
13
14
15
16
17
18
19
20
21
22
23
24
25
26
27
28
29
30
31
32
33
34
35
36
37
38
39
40
41
42
43
44
45
46
47
48
49

1
2
3
4
5
6
7
8
9
10
11
12
13
14
15
16
17
18
19
20
21
22
23
24
25
26
27
28
29
30
31
32
33
34
35
36
37
38
39
40
41
42
43
44
45
46
47
48
49

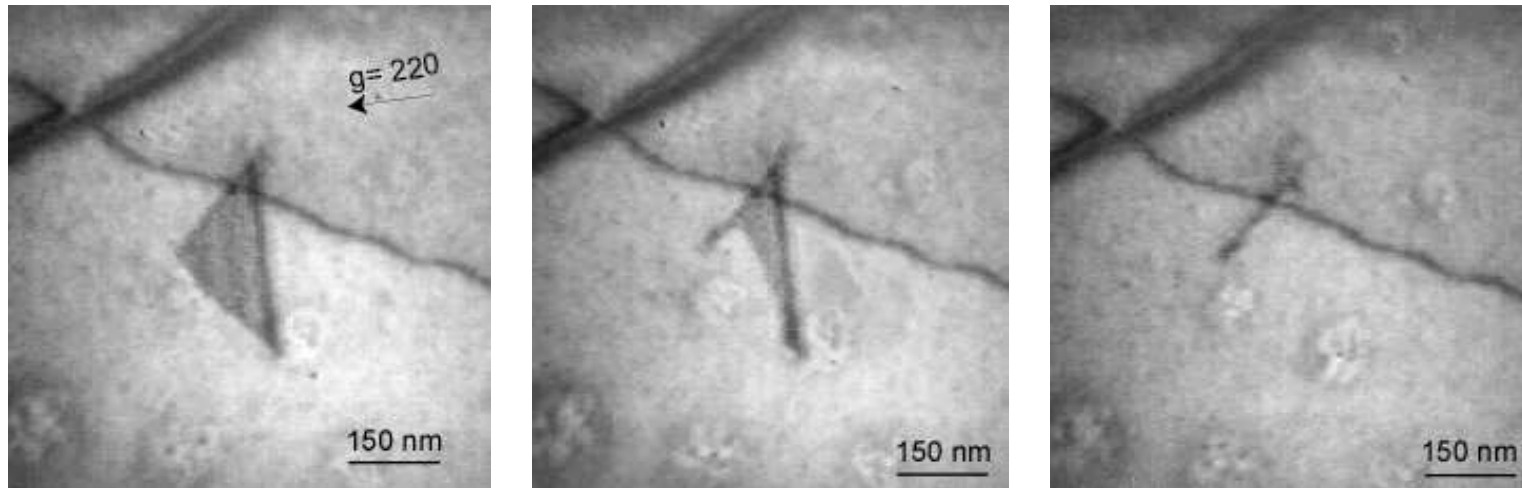


Figure 6

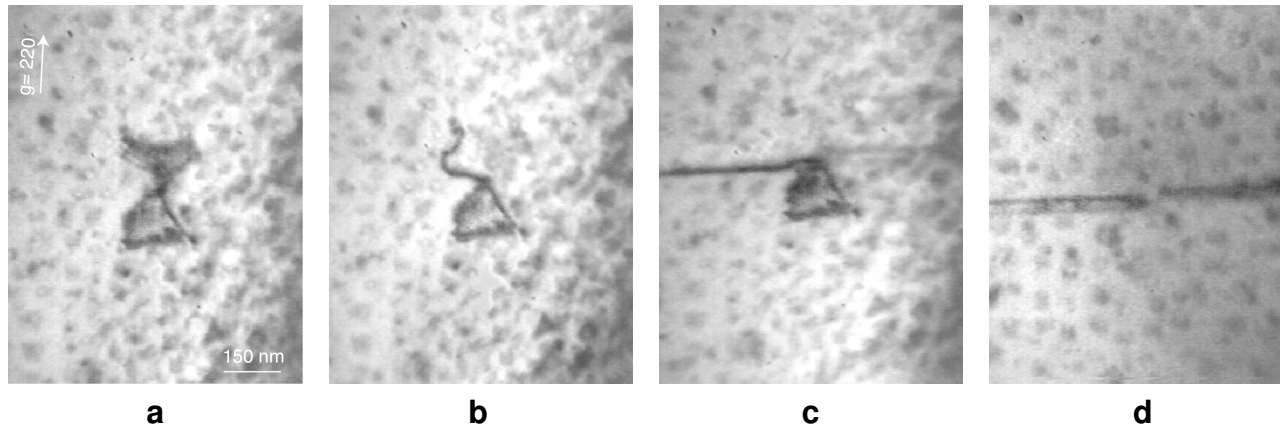


Figure 7

1
2
3
4
5
6
7
8
9
10
11
12
13
14
15
16
17
18
19
20
21
22
23
24
25
26
27
28
29
30
31
32
33
34
35
36
37
38
39
40
41
42
43
44
45
46
47
48
49

1
2
3
4
5
6
7
8
9
10
11
12
13
14
15
16
17
18
19
20
21
22
23
24
25
26
27
28
29
30
31
32
33
34
35
36
37
38
39
40
41
42
43
44
45
46
47
48
49

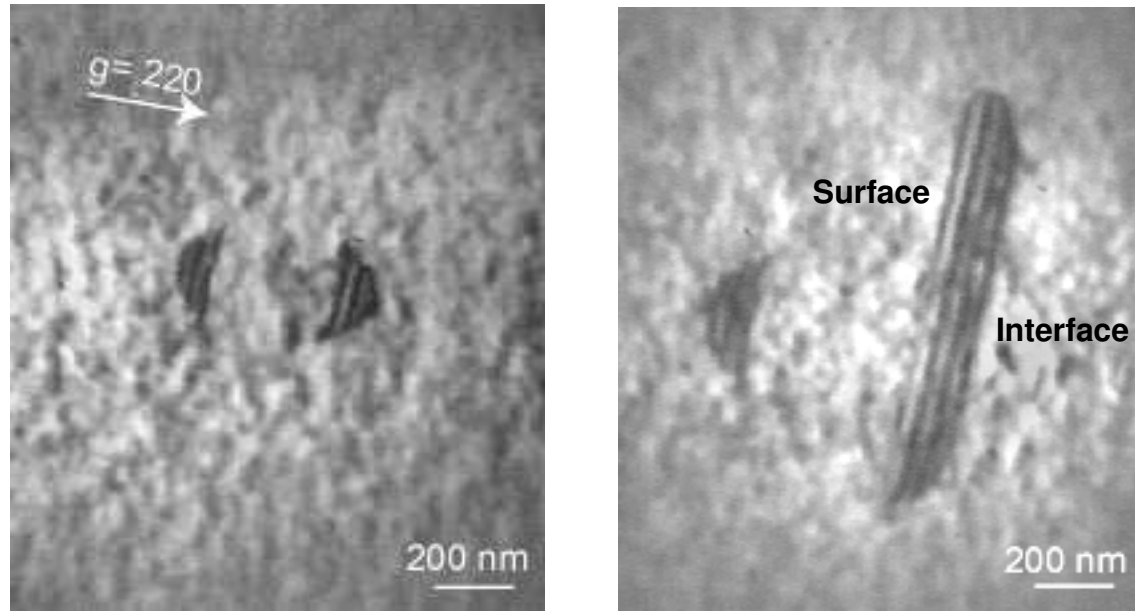


Figure 8

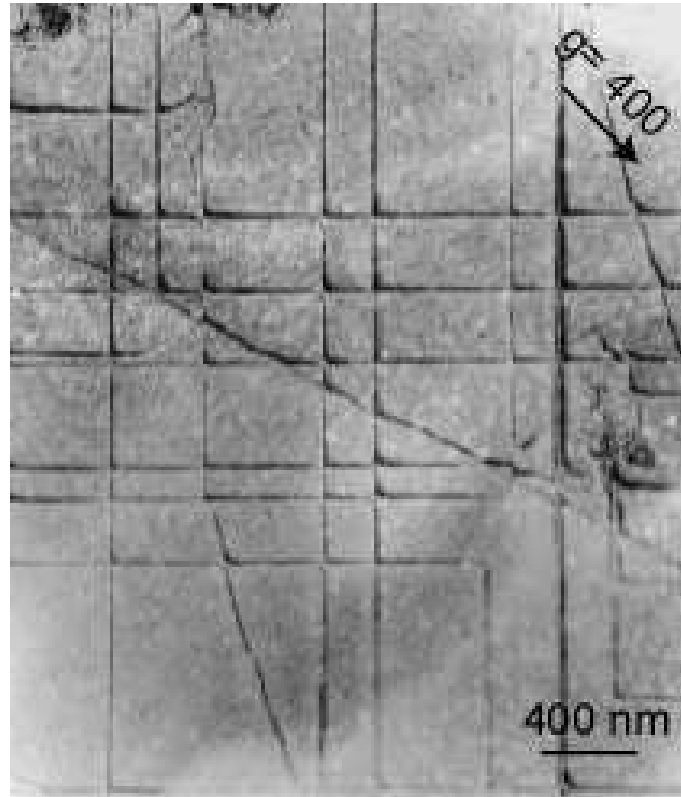


figure 9a

1
2
3
4
5
6
7
8
9
10
11
12
13
14
15
16
17
18
19
20
21
22
23
24
25
26
27
28
29
30
31
32
33
34
35
36
37
38
39
40
41
42
43
44
45
46
47
48
49

1
2
3
4
5
6
7
8
9
10
11
12
13
14
15
16
17
18
19
20
21
22
23
24
25
26
27
28
29
30
31
32
33
34
35
36
37
38
39
40
41
42
43
44
45
46
47
48
49

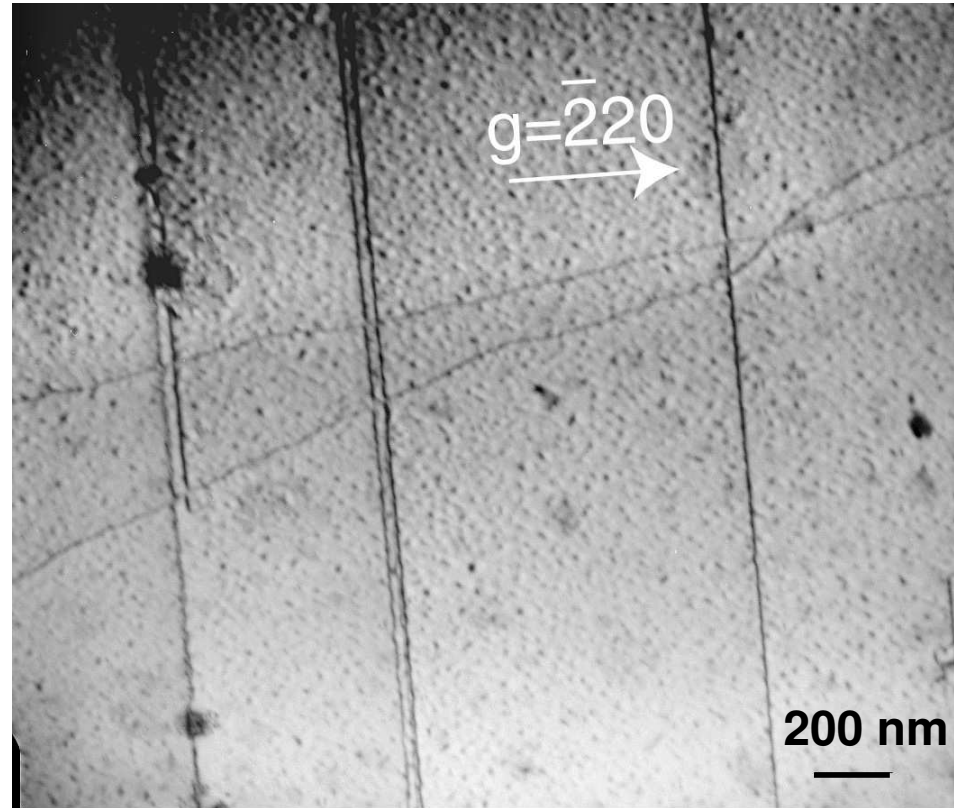


Figure 9b

1
2
3
4
5
6
7
8
9
10
11
12
13
14
15
16
17
18
19
20
21
22
23
24
25
26
27
28
29
30
31
32
33
34
35
36
37
38
39
40
41
42
43
44
45
46
47
48
49

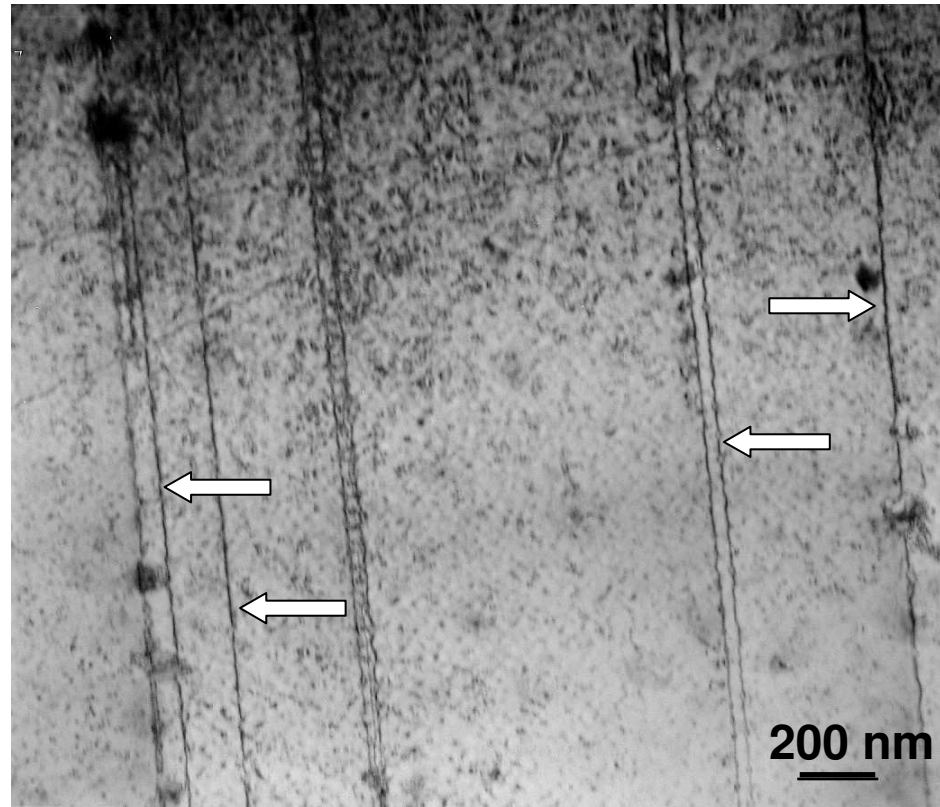


Figure 9b (contd)